

Tightness of slip-linked polymer chains

Ralf Metzler,^{1,2} Andreas Hanke,^{1,3} Paul G. Dommersnes,^{1,4} Yacov Kantor,^{5,1} and Mehran Kardar¹

¹*Department of Physics, Massachusetts Institute of Technology,
77 Massachusetts Avenue, Cambridge, Massachusetts 02139, USA*

²*NORDITA, Blegdamsvej 17, DK-2100 København Ø, Denmark*

³*Department of Physics, Theoretical Physics, 1 Keble Road, Oxford OX1 3NP, United Kingdom*

⁴*Department of Physics, Norwegian University of Science and Technology, N-7491 Trondheim, Norway*

⁵*School of Physics and Astronomy, Sackler Faculty of Exact Sciences, Tel Aviv University, Tel Aviv 69978, Israel*

(Dated: 25th October 2018)

We study the interplay between entropy and topological constraints for a polymer chain in which sliding rings (*slip-links*) enforce pair contacts between monomers. These slip-links divide a closed ring polymer into a number of sub-loops which can exchange length between each other. In the ideal chain limit, we find the joint probability density function for the sizes of segments within such a slip-linked polymer chain (*paraknot*). A particular segment is tight (small in size) or loose (of the order of the overall size of the paraknot) depending on both the number of slip-links it incorporates and its competition with other segments. When self-avoiding interactions are included, scaling arguments can be used to predict the statistics of segment sizes for certain paraknot configurations.

PACS numbers: 05.20.-y, 02.10.Kn, 87.15.-v, 82.35.Lr

I. INTRODUCTION

Topological constraints decrease the accessible degrees of freedom of a polymer chain [1]. Whether temporary or permanent, they are quite ubiquitous and effect the typical behaviour of polymers. For instance, temporary entanglements between chains in a solution or melt of polymers give rise to reptation dynamics as described by the tube model [2, 3]. Permanent entanglements, in turn, are central for the elastic behaviour of rubber (where they are chemically induced during vulcanisation) [4], gels and Olympic gels [2]. Their influence on the dynamics is reflected by broad relaxation time spectra [5].

Knots are a particular form of permanent topological entanglements: A “knotted” closed chain cannot be reduced to a simple ring (the so-called unknot) without breaking bonds [6, 7, 8, 9]. One of the few exact results pertaining to the statistics of knots is that a sufficiently long closed self-avoiding walk contains knots with probability one [10, 11]. Thus, topological constraints are inevitably created during the polymerisation of long closed chains and, more generally, knots and permanent entanglements are a ubiquitous feature of multi-chain polymer melts and solutions.

Topological considerations also play a major role in numerous biological and chemical systems. For example, the chromosomes forming almost two metres of tangled, knotted DNA cannot be separated during mitosis, and the genetic code of the DNA double helix cannot be fully accessed during transcription, in the presence of knots [12, 13, 14]. Special enzymes, namely DNA topoisomerases, are necessary to actively remove knots and entanglements under consumption of energy from ATP [12, 13, 14, 15, 16]. The interplay between energy and entropy at a fixed topology is relevant to the secondary structure of RNA which consists of paired segments interrupted by open loops acting as entropy source

[17, 18]. Similar issues arise in the helix-coil transition of DNA [19, 20, 21, 22]. Knotted configurations have even been found in some proteins [23, 24]. Dynamically, the presence of knots and their possible effects on the mobility of biopolymers are essential to the understanding of their behaviour *in vivo* or, e.g., as studied by electrophoresis *in vitro* [25]. A similar role is played by topological effects for the translocation of viral and non-viral proteins [12, 26], and packaging of DNA [27]. In supramolecular chemistry, molecules with identical bond sequence but different topology can be produced which exhibit different physical properties, and mechanically linked molecules open up new vistas in information processing or nano-engineering [28, 29, 30]. Further interest in the theoretical study of the equilibrium behaviour of polymers with a fixed topology arises from new experimental techniques by which single molecules can be probed and manipulated [31, 32, 33, 34], providing information on the mechanical behaviours of knotted and unknotted biopolymers [35, 36, 37].

Mathematical studies of topological structures date back to Kepler [38], Euler [39] and Listing [40]. Motivated by Thomson’s theory of vertex atoms [41], systematic studies of knots were undertaken by Tait, Kirkwood and Little [42, 43, 44, 45]. Knot theory provides a number of so-called knot invariants by means of which knots can be classified, such as the Gauss winding number, the number of essential crossings, or more refined invariants like knot polynomials [7, 8, 9]. All permitted configurational changes of a knot can be decomposed into the three Reidemeister moves [7, 8, 9]. There exists a fundamental relation between knots and gauge theory as knot projections and Feynman graphs share the same basic ingredients corresponding to a Hopf algebra [8].

Recently there has been increasing interest in the interplay of topological constraints and thermal fluctuations; the latter being ubiquitous for dilute or semidilute poly-

mer solutions or melts at finite temperatures. Statistical mechanical treatments of permanent entanglements and of knots are, however, quite difficult since topological restrictions cannot be formulated as a Hamiltonian problem but appear as hard constraints partitioning the phase space [2, 6, 46, 47, 48]. Consequently, only a relatively small range of problems have been treated analytically (see, for instance, [49, 50, 51, 52, 53, 54, 55, 56, 57]).

To overcome such difficulties in the context of the entropic elasticity for rubber networks, Ball, Doi, Edwards and coworkers replaced permanent entanglements by slip-links [58]. Slip-links enforce contacts between pairs of monomers but the chain can slide freely through them. Surrogate networks containing slip-links have been successful in the prediction of important physical quantities of rubber networks [59]. In a similar fashion, we investigate the statistical behaviour of single polymer chains in which a fixed topology is created by a number of slip-links. Such “*paraknots*” can be studied analytically using known results for Gaussian random walks in the ideal chain limit [3, 50, 60]. In the language of graphs, slip-link contacts represent vertices with four outgoing legs, enabling us to make use of a scaling approach to determine the leading behaviour in the presence of self-avoiding interactions. The paraknot approach thus complements our previous study of *flat* knots in which such vertices correspond to crossings [61].

In the following section, we start with a brief summary of conflicting answers to the question of whether the topological details in a knotted polymer are localised within a small portion of the chain, and thus segregated from an unentangled segment. We then introduce the concept of paraknots to study localisation effects for polymers with fixed topology. Paraknots are first analysed for ideal chains in Section III A; various contributions to the joint probability density function (PDF) of segment sizes are easily separated in this case. There is no similar factorisation of the PDF for self-avoiding segments, but as discussed in Section III B, scaling arguments can be used to infer the limiting behaviour of the PDF as one or more segments contract to small size. The question of the relative sizes of segments in a paraknot is taken up in Section IV. By analysing the behaviour of the unconditional PDF of a particular segment at small sizes we can infer whether the segment has the tendency to be tight. Yet, to describe the actual probability of finding a tight segment, one must consider the competition between all segments. For example, even in cases where all segments prefer to be tight *per se*, a given segment can still have a finite probability of being loose.

II. FROM KNOTS TO PARAKNOTS

In Fig. 1a we depict the projection of a trefoil knot in a symmetric (bottom) and an asymmetric configuration (top). In the latter case, we can introduce a knot region that part of the knot which contains all topological

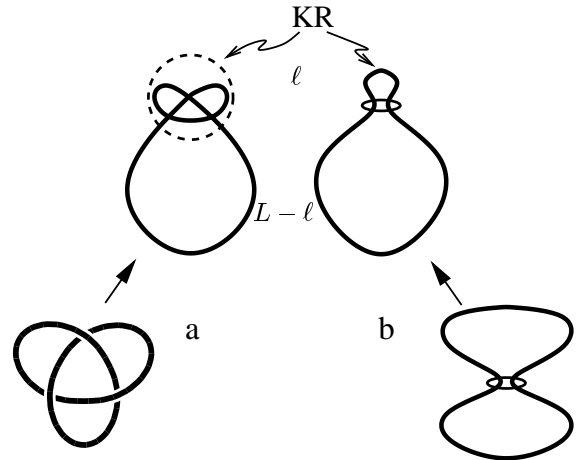


Figure 1: Depiction of the knot region (KR) for (a) a trefoil knot and (b) a figure-eight structure in which a slip-link enforces a pair contact (compare Fig. 2). In both cases, a symmetric and an asymmetric configuration are shown. The size of the KR is termed ℓ and the length of the remaining simply connected chain is $L - \ell$.

details except for the one larger simply connected segment, as indicated by the dashed line. Initial indications of tight knotted regions are implicit in 3D Monte Carlo simulations of Janse van Rensburg and Whittington [62], who studied the mean extension of the unknot and several knot types up to six essential crossings. They found that in the scaling form $R_g^2 \sim (A + BL^{-\Delta})L^{2\nu}$ of the gyration radius both the prefactor A and the exponent ν in the leading contribution are *independent* of the knot type [62]. In fact, ν was found to be consistent with the known value $\nu = 0.588$ of the swelling exponent of a ring polymer [2, 6]. (The confluent correction term was estimated to decay with $\Delta \approx 1/2$.) Conversely, employing a Flory-type argument under the assumption that the knot is equally *spread out* over the polymer, Quake predicted that the gyration radius should contain the scaling dependence $R_g \sim \tilde{A}C^{1/3-\nu}L^\nu$ on the number of essential crossings C in the leading order term, i.e., that the amplitude of R_g decreases with increasing knot complexity [53]. This result was supported by his numerical study of knots up to 81 [53], with a different algorithm than used in Ref. [62]. Grosberg *et al.* [54] also make use of a Flory-type approach assuming that in an evenly delocalised knot the topological constraints can be replaced by a tube whose radius can be determined from the aspect ratio of a maximally inflated state. They obtained similar conclusions to Quake, although they also remark that thermodynamically a segregation into a simply connected ring polymer and a dense knot region might occur [54]. In a later work, Grosberg states that a more powerful approach is needed to theoretically decide between the two options [52]. More recent numerical studies seem to corroborate the independence of the gyration radius of the knot type in long enough polymers. Thus, in 3D

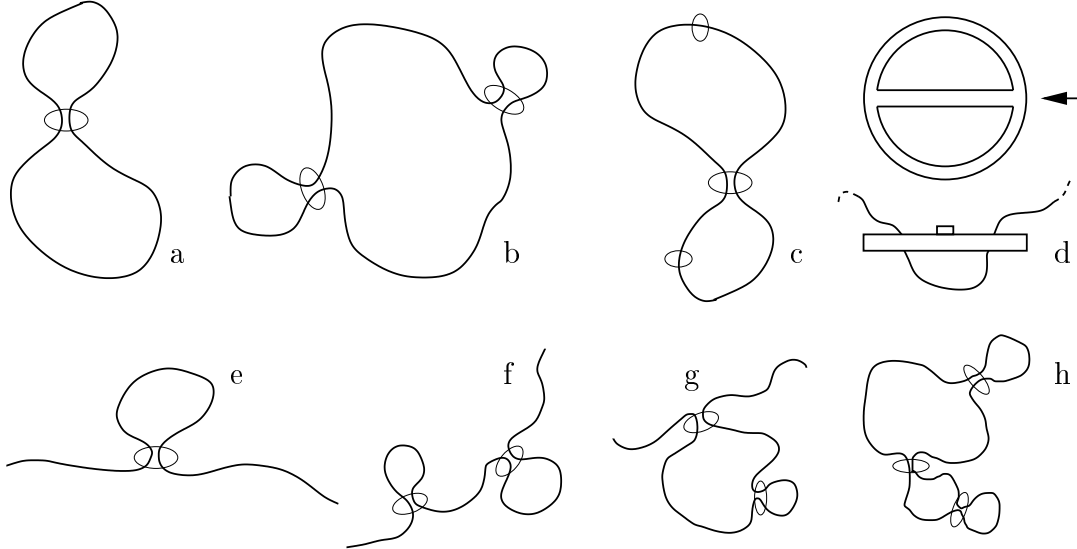


Figure 2: A collection of different paraknots discussed in the text. (a) The figure-eight paraknot is formed by placing a slip-link on a ring polymer. (b) The next higher order paraknot with two slip-links. (c) The figure-eight paraknot with two additional sliding rings, one on each separated loop. (d) Visualisation of a slip-link: the belt buckle shape allows the chain to slide freely through the slip-link without retracting entirely. The lower part corresponds to the view from right as indicated by the arrow. (e) The lowest order open paraknot. (f) Open paraknot with two slip-links. (g) Topologically different configuration with two slip-links. (h) Paraknot necklace with three slip-links.

Orlandini *et al.* calculate in a Monte Carlo study the number of configurations ω_K of different knot types K , reporting that $\omega_K \sim \mu^L L^{\alpha-3}$ where both μ and α are independent of K for prime knots, and that an additional factor L^{n-1} occurs for composite knots with n prime components [63]. These authors conclude that one or more tight knot regions can move along the perimeter of a simply connected ring polymer, each prime component being represented by one knot region [63]. An analogous result was obtained in 2D by Guitter and Orlandini [64]. Consistent with these findings, Katritch *et al.* obtained that the knot region is tight in 3D with a relatively high probability [65]. The investigations of Shimamura and Deguchi [66] corroborate this picture in obtaining that the gyration radius is independent of the knot type in some limit of their model.

Why should knots be confined to a small region of the polymer? Entropic effects give rise to long-range interactions as we demonstrate for the figure-eight structure sketched in Fig. 1b in which a permanent pair contact is enforced by a slip-link, creating two loops of lengths ℓ and $L - \ell$, which can freely exchange length. In the ideal chain limit, the two loops correspond to returning random walks, i.e., the PDF $p(\ell)$ for the size ℓ becomes [2, 67]

$$p_{\text{id}}(\ell) \propto \ell^{-d/2} (L - \ell)^{-d/2}, \quad (1)$$

where d is the embedding dimension. The average loop size $\langle \ell \rangle = \int_a^{L-a} d\ell \ell p(\ell)$, where a is a short-distance cutoff

set by the lattice constant, is trivially $\langle \ell \rangle = L/2$, due to the symmetry of the structure. However, as the PDF is strongly peaked at $\ell = 0$ and $\ell = L$, a *typical* shape consists of one small (*tight*) and one large (*loose*) loop. For instance, in $d = 3$ the mean size of the smaller loop $\langle \ell \rangle_<$ scales as

$$\langle \ell \rangle_< \sim a^{1/2} L^{1/2}, \quad d = 3, \quad (2)$$

which corresponds to *weak localisation* in the sense that the smaller loop still grows with L , but with an exponent smaller than one. By comparison, for $d > 4$ one encounters $\langle \ell \rangle_< \sim a$, corresponding to *strong localisation* as the size of the smaller loop does not depend on L but is set by the short-distance cutoff a . On the other hand, for $d = 2$ one finds $\langle \ell \rangle_< \sim L/|\ln(a/L)|$, such that the smaller loop is still rather large. However, we will see in the next section that this is no longer true if we include self-avoiding interactions for the chains; in that case, the localisation for $d = 2$ is even stronger than for $d = 3$.

Equation (2) shows that the smaller loop, of length ℓ , of the figure-eight structure is indeed tight in $d = 3$. In fact, for *flat* knots rendered as quasi 2D knot projections, it turns out that *all* prime knots become tight, and that their leading scaling behaviour corresponds to the figure-eight structure [61]. This localisation is the consequence of a delicate interplay between competing effects. Statistically, the confinement of topological details into a localised region of the polymer chain is favoured entropically as then the topological constraints act on a small

portion of the chain, exclusively, and the remaining major part has access to all degrees of freedom of a simply connected ring polymer. This tendency towards confinement is counteracted by the internal degrees of freedom of the knot region in which the substructures can exchange length among each other. It turns out that the tradeoff is in favour of localisation.

We propose that slip-link structures grasp some essential features of the statistical behaviour of real knots and therefore call them *paraknots*. Some elementary examples of paraknot structures which will be discussed in the following Sections are displayed in Fig. 2. The slip-links in these configurations can be viewed as little rings which enforce pair contacts within the chain such that the loop formed by the slip-link is not allowed to fully retract. In a simulation, this latter property can be included by a belt buckle shape as sketched in Fig. 2d. In a paraknot, one or several loops may be cut, creating open chain segments as in Figures 2e to g. Such “open” paraknot types can be stabilised (i.e., an open end prevented from escaping through a slip-link) by attaching “stoppers” to the open ends, such as latex microspheres, ring-molecules, or C_{60} balls, as known from supramolecular chemistry [29, 30].

Paraknots are tractable exactly in the ideal chain limit, and by scaling theories in the self-avoiding domain. In the following, we investigate the statistical description and the localisation properties of several paraknot structures.

III. STATISTICAL WEIGHTS OF PARAKNOT STRUCTURES

A general paraknot can be constructed, as shown in Fig. 3, from an arc diagram similar to those used to classify the secondary structure of RNA [17, 18]. Such an arc diagram is the blueprint of the associated paraknot, and it features the original loop into which slip-links are introduced by connecting pairs of monomers through the dashed lines. To simplify the analysis, we only consider paraknots with unconcatenated loops, i.e., the arcs are not allowed to intersect each other. In the RNA language, this means that pseudoknots are not permitted [17, 18]. With this restriction, the joint PDF for the sizes of various segments simplifies to a product of contributions from loops, in the case of ideal (Gaussian) polymers. As discussed next, in the case of self-avoiding walks, only scaling information is available in the limit when segments contract to small sizes.

A. Ideal chains

For ideal chains, analytical calculations are rather straightforward for non-crossing arc diagrams (similar to Hartree graphs). For instance, consider the paraknot shown in Fig. 3 for fixed loop lengths ℓ_1, \dots, ℓ_5 . The key observation is that for ideal chains the degrees of freedom

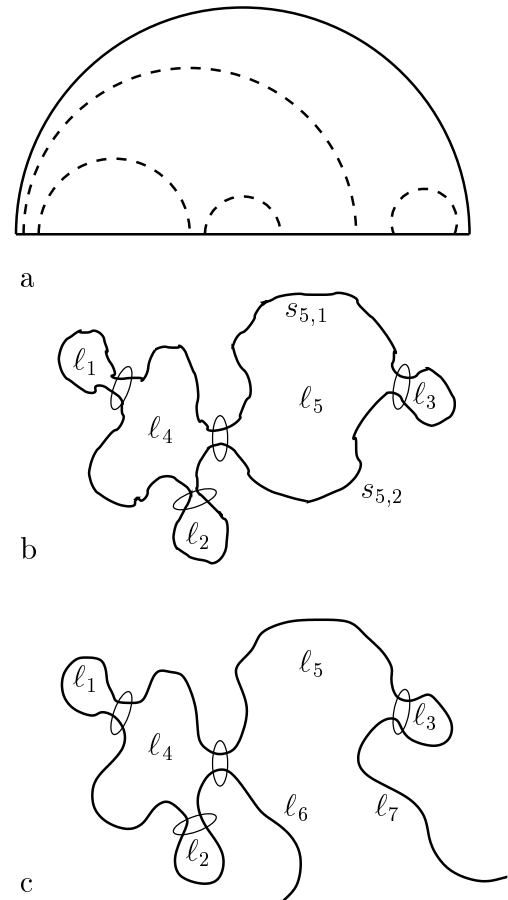


Figure 3: (a) Arc diagram for the construction of a closed paraknot from a polymer ring (full line). The dotted lines indicate which points of the chain are connected to each other by slip-links. (b) The paraknot resulting from this procedure. (c) Open paraknot obtained by cutting loop 5, creating two open legs. Note that individual connectors (dashed lines) are not allowed to intersect each other, i.e., the paraknot contains unconcatenated loops.

associated with the individual loops are decoupled from one another, so that the PDF of the paraknot factorises into the corresponding loop contributions. Following the above example, a general paraknot \mathcal{P} can be described by the set $\{\ell_1, \ell_2, \dots, \ell_m\}$ of individual loop lengths (also including end-to-end lengths in case of linear segments) under the constraint $L = \sum_i \ell_i$, where the contributions from the individual loops (or linear segments) factorise. In equilibrium, these lengths are thus distributed according to the joint PDF

$$p_{\mathcal{P}}(\ell_1, \ell_2, \dots, \ell_m) \propto \delta \left(L - \sum_{i=1}^m \ell_i \right) \prod_{i=1}^m \ell_i^{-\theta_i}, \quad (3)$$

where the exponents θ_i are constructed from the following contributions [68]:

(i) Connectivity factor: This factor accounts for the configurational entropy of a given loop (or linear seg-

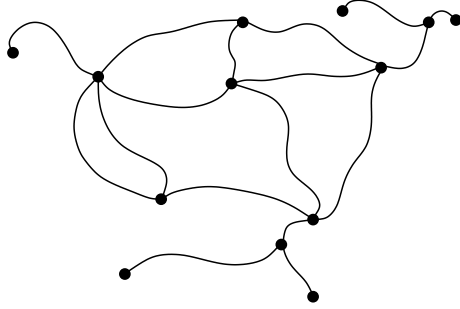


Figure 4: Polymer network \mathcal{G} with vertices (•) of different order ($n_1 = 5$, $n_3 = 4$, $n_4 = 3$, $n_5 = 1$).

ment) of length ℓ . For a loop, the connectivity factor follows from the return probability of a Gaussian random walk, which is $\sim \ell^{-d/2}$. The absence of any constraint for a linear segment corresponds to a factor $\sim \ell^0$.

(ii) Sliding entropy: A given loop (or linear segment) of length ℓ has additional degrees of freedom associated with the slip-links which slide on it. This is due to the relative motion of these slip-links along the segment. The presence of n slip-links on a loop (or linear segment) thus leads to a factor of $\ell^{n-1}/(n-1)!$ (or $\ell^n/n!$). Additional degrees of freedom in the form of sliding rings confined to a given segment as depicted in Fig. 2c enter the PDF analogously.

(iii) Energetic factors: If an external force is applied to the paraknot, a Boltzmann weight enters the expression for the size distribution. For instance, if an open paraknot is pulled with a constant force \mathbf{f} , this weight corresponds to the average $\overline{\exp\{\beta\mathbf{f} \cdot \mathbf{r}\}} = \exp\{\beta^2 f^2 \overline{r^2}/(2d)\}$ where the overline indicates the average over all end-to-end distances \mathbf{r} of the backbone segment, and $\beta \equiv 1/(k_B T)$. (Such effects will be relegated to a future work [69].)

B. Self-avoiding chains

If self-avoiding constraints for the chains are included, the above reasoning for ideal chains, in particular the factorisation of the PDF, is no longer valid in general since now every loop or segment of the paraknot interacts with all the others. However, progress can be made, allowing for quantitative predictions of the leading scaling behaviour of a given paraknot, by employing the scaling theory for self-avoiding polymer networks developed by Duplantier [70], Schäfer *et al.* [71], and Ohno and Binder [72]. This approach has recently been applied to the study of DNA denaturalisation by Kafri *et al.* [20, 21] and to the study of 2D knots [61].

A general polymer network \mathcal{G} like the one depicted in Fig. 4 consists of a number of vertices which are joined by \mathcal{N} chain segments of individual lengths $s_1, \dots, s_{\mathcal{N}}$ whose total length is $L = \sum_{i=1}^{\mathcal{N}} s_i$. The number of configura-

tions of such a network scales as [70, 71, 72]

$$\omega_{\mathcal{G}} \sim \mu^L s_{\mathcal{N}}^{\gamma_{\mathcal{G}}-1} \mathcal{Y}_{\mathcal{G}} \left(\frac{s_1}{s_{\mathcal{N}}}, \dots, \frac{s_{\mathcal{N}-1}}{s_{\mathcal{N}}} \right), \quad (4)$$

where μ is the effective connectivity constant for self-avoiding walks and $\mathcal{Y}_{\mathcal{G}}$ is a scaling function. The topology of the network is reflected in the exponent

$$\gamma_{\mathcal{G}} = 1 - d\nu\mathcal{L} + \sum_{N \geq 1} n_N \sigma_N, \quad (5)$$

where $\mathcal{L} = \sum_{N \geq 1} (N-2)n_N/2 + 1$ is the number of independent loops, n_N is the number of vertices with N legs, and σ_N is an exponent connected to an N -vertex. The PDF of the paraknot then follows from the number of configurations $\omega_{\mathcal{G}}$ by normalisation with respect to the variable segment lengths.

(i) Connectivity factor: To illustrate how the connectivity factors (of the form $\sim \ell^{-d/2}$ and $\sim \ell^0$ for closed loops and linear segments in the Gaussian case) are modified, let us consider the cases of the figure-eight paraknot (Fig. 2a), and its open counterpart (Fig. 2e).

The figure-eight paraknot corresponds to a network with two loops of lengths ℓ and $L - \ell$, respectively, and one vertex with 4 legs. We thus obtain

$$\omega_8 \sim \mu^L (L - \ell)^{-2d\nu + \sigma_4} \mathcal{Y}_8 \left(\frac{\ell}{L - \ell} \right), \quad (6)$$

for the configuration number. Now we use the *a priori* assumption that $L - \ell \gg \ell$. Then, the large loop should behave like a ring polymer of length $L - \ell$, i.e., it should contribute to $\omega_{\mathcal{G}}$ in the scaling form $(L - \ell)^{-d\nu}$ [20]. This can only be fulfilled if the scaling function behaves like $\mathcal{Y}_8(x) \sim x^{-c}$ with $c = d\nu - \sigma_4$. The final result for the number of configuration of the self-avoiding figure-eight paraknot then becomes

$$\omega_8 \sim \mu^L (L - \ell)^{-d\nu} \ell^{-d\nu + \sigma_4}. \quad (7)$$

In $d = 2$, with $\nu = 3/4$ and $\sigma_4 = -19/16$ [20, 70, 71], we therefore find that the small loop scales like ℓ^{-c} where $c = 2.6875$. In $d = 3$, we obtain the exponent $c \approx 2.24$ using $\nu = 0.588$ and $\sigma_4 \approx -0.46$ [20, 70, 71, 73]. The strong localisation which obtains for both $d = 2$ and $d = 3$ is the *a posteriori* justification of the $L - \ell \gg \ell$ assumption, and the procedure is therefore self-consistent. Note that in the presence of self-avoiding constraints, the localisation is stronger in 2D than in 3D, in contrast to the ideal chain case (see Sec. II).

We performed a Monte Carlo analysis of the elementary slip-link in 2D with a standard bead-and-tether chain. In Fig. 5a, we show the equilibration of a symmetric initial configuration and its fluctuations as a function of Monte Carlo steps. Clearly, the separation into two length scales is fast and fluctuations are relatively small. The size distribution of the small loop is displayed in Fig. 5b. From the plot, we realise that the scaling be-

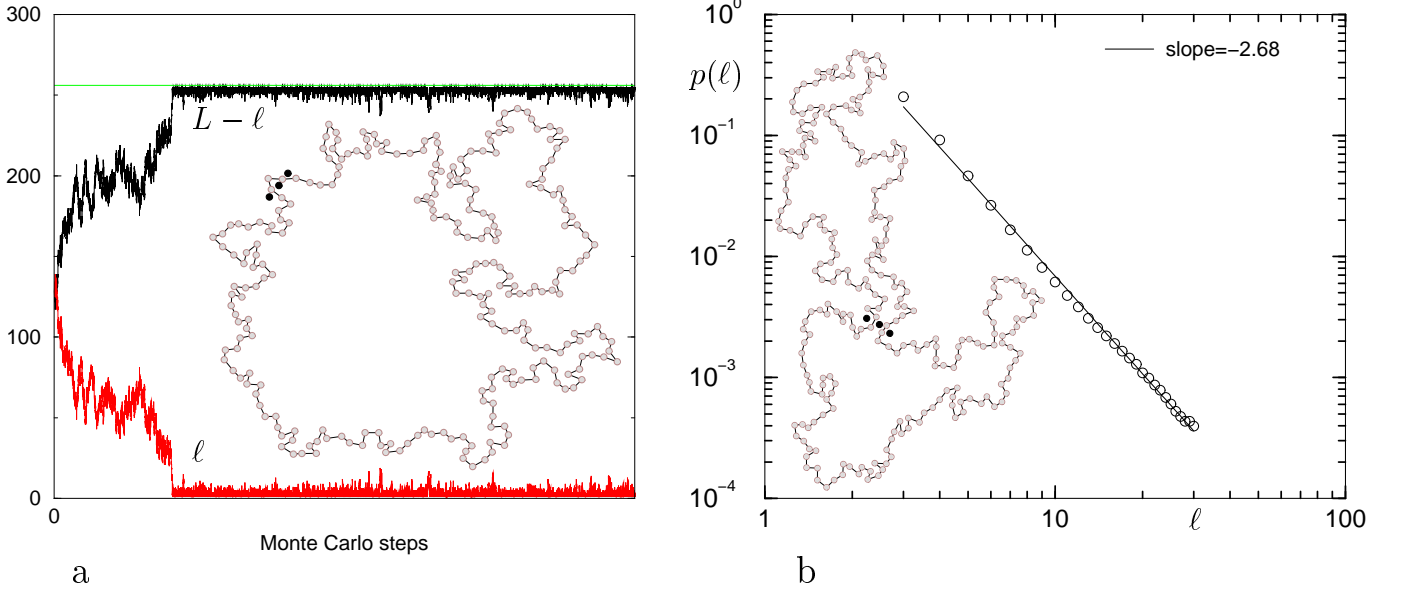


Figure 5: Monte Carlo simulation of a figure-eight paraknot in 2D. (a) Loop sizes ℓ and $L - \ell$ as a function of Monte Carlo steps for 256 monomers. In the inset, a typical equilibrium configuration is shown. The slip-link is made up of the three tethered beads rendered black which constitute the 2D version of the belt buckle shape depicted in Fig. 2d. (b) Probability density for the size ℓ of the smaller loop for a figure-eight with 512 monomers. The inset shows an intermediate configuration reminiscent of the symmetric initial condition.

haviour is surprisingly well fulfilled, and that the predicted value is reproduced in good agreement. This result was corroborated experimentally for a figure-eight necklace chain on a vibrating plate [74].

Compare this finding to the lowest order open paraknot (o) sketched in Fig. 2e. Apart from the vertex with 4 legs, there are two vertices with one leg, one for each of the two ends of the linear chain segment, thus yielding

$$\omega_o \sim \mu^L (L - \ell)^{1-d\nu+2\sigma_1+\sigma_4} \mathcal{Y}_o \left(\frac{\ell}{L - \ell} \right). \quad (8)$$

We again assume *a priori* that the open chain segment is the overall dominating structure of size $L - \ell$. It thus enters into ω_o in the form $(L - \ell)^\gamma$ where $\gamma = 2\sigma_1 + 1$ is the configuration exponent [50, 70, 75], which implies

$$\omega_o \sim \mu^L (L - \ell)^\gamma \ell^{-d\nu+\sigma_4}. \quad (9)$$

Thus, we find the same loop closure exponent as for the figure-eight structure above [see Eq. (7)]. This is not surprising, as the small loop is statistically independent of the large structure; in other words, the topological exponent σ_4 stems from the nature of the vertex, which is a *local* quantity.

The closure factor for a loop in such simple geometries as the figure-eight or the lowest order open paraknot is therefore given by $\sim \ell^{-d\nu+\sigma_4}$; the factor for the degrees of freedom of the linear chain segment in the latter enters as $\sim (L - \ell)^\gamma$.

(ii) Sliding entropy: Consider the paraknot shown in Fig. 3b. It constitutes a polymer network \mathcal{G} in which

four 4-vertices (corresponding to the slip-links) are joined by a number of chain segments s_i with $\ell_1 = s_1$, $\ell_5 = s_{5,1} + s_{5,2}$, etc. Since the loops are non-concatenated, it is possible to integrate the right hand side of Eq. (4) for *fixed* loop lengths ℓ_1, \dots, ℓ_5 over some of the segment lengths s_i in such a way that the resulting expression depends on the loop lengths only, i.e.,

$$\omega_{\mathcal{G}}^{(\ell)} \sim \mu^L \ell_1^{\gamma_{\mathcal{G}}-1} \ell_4^2 \ell_5 \mathcal{X}_{\mathcal{G}} \left(\frac{\ell_1}{\ell_5}, \dots, \frac{\ell_4}{\ell_5} \right), \quad (10)$$

where the scaling function $\mathcal{X}_{\mathcal{G}}$ depends on ratios of loop lengths (again, this procedure would not be possible if the paraknot contained concatenated loops). The superscript (ℓ) on $\omega_{\mathcal{G}}$ indicates that here the loop lengths ℓ_1, \dots, ℓ_5 are fixed. The factors of ℓ_4^2 and ℓ_5 in the above expression correspond to the sliding entropy already encountered for ideal chains, see (ii) in Sec. III A.

IV. TIGHT OR LOOSE

When is a certain segment of such a paraknot network tight? *A priori*, this can be investigated by integration of the joint PDF over all other segments. The result depends on both the local property of the segment itself, i.e., on its exponent in the joint size distribution, and its global interplay with other segments in the paraknot in their cooperative search for the entropically favoured configuration. In practice, the unconditional PDF can only be obtained for Gaussian paraknots in which the joint

PDF has the multiplicative form in Eq. (3). Such calculations are not possible for general self-avoiding paraknots, as the unconditional PDF comes out from the specific scaling analysis for a given paraknot configuration. We therefore address phantom and self-avoiding cases separately.

A. Ideal chains

Consider the joint PDF in Eq. (3) for a given paraknot \mathcal{P} with \mathcal{N} segments. According to the previous section, the exponents θ_i in Eq. (3) are given by $\theta_i = d/2 - (n_i - 1)$ if ℓ_i is a loop or by $\theta_i = -n_i$ if it is a linear segment, where n_i is the number of slip-links and sliding-rings connected to this segment. From Eq. (3), we consider a segment to be loose *per se* if its exponent $\theta_i \leq 1$, otherwise it is tight (and “super-tight” if $\theta_i > 2$). We can now distinguish between three different global situations:

(i) There is one loose segment and all others are tight. This case occurs if in \mathcal{P} only one segment with $\theta_{\mathcal{N}} \leq 1$ exists, while all others have $\theta_i > 1$.

(ii) There is more than one loose segment and possibly some tight segments. In this case, the loose segments compete for the length L . On the average, if there are \mathcal{M} loose segments, the characteristic length of any specific segment is $\langle \ell_j \rangle = \frac{1-\theta_j}{\sum_{i=1}^{\mathcal{M}} (1-\theta_i)} L$, which is always larger than 0 and smaller than L . The ratio of characteristic lengths for a pair of segments j, k is then given by $\langle \ell_j \rangle : \langle \ell_k \rangle = (1 - \theta_j) : (1 - \theta_k)$ [76].

(iii) All segments are tight *per se* in the sense that all $\theta_i > 1$. In this case, a symmetry-breaking occurs and one segment becomes large. The unconditional PDF for each segment will have two peaks corresponding to tight or loose configurations.

In a paraknot which contains one or multiple open segments, the open segments are always loose and therefore only cases (i) and (ii) can arise: Depending on the exponents of the closed loops in such a structure, these loops may either be loose or tight. Note that cases (i) and (iii) exhibit one large loop, in (i) this is the loose segment and in (iii) it is the one segment which becomes large by symmetry breaking. As all other segments of paraknots which belong to these classes are tight, the gyration radius of such paraknots is, to leading order, the same as for an unknot of length L . For paraknots belonging to class (ii), segments of comparable size make up the gyration radius. Depending on the details of the structure, the gyration radius should be given by similar expressions to those developed in Refs. [6, 53]. Thus, the gyration radius decreases with increasing number of loose segments.

B. Self-avoiding chains

As mentioned, generalising the previous classification to self-avoiding structures is not straightforward. Let

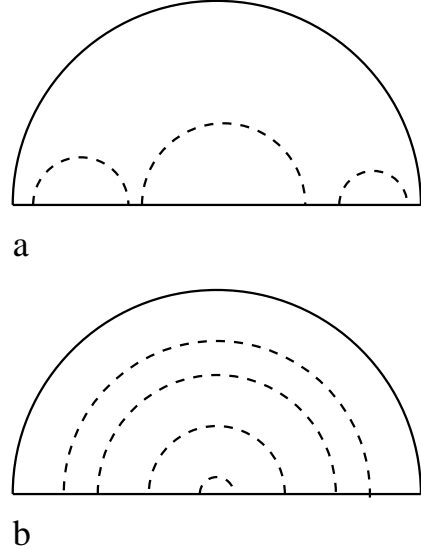


Figure 6: Arc diagram for (a) the Round Table configuration with $n = 3$ fringe loops, and (b) the Necklace paraknot.

us therefore consider the tightness of segments in a self-avoiding paraknot by means of three examples.

1. The Round-Table Configuration

This configuration corresponds to arc diagrams in which none of the connecting arcs is located inside another arc, as shown in Fig. 6a. The resulting paraknot features a number n of loops located at the fringe of a central loop, as depicted to lowest order in Fig. 2b. As the loops are independent and are connected to one slip-link each, they enter the joint PDF of loop sizes through the loop closure factor $\sim \ell_i^{-d\nu + \sigma_4}$ as was found for the figure-eight paraknot. They are therefore super-tight for self-avoiding chains. Conversely, the central loop has access to additional degrees of freedom stemming from the relative motion of the slip-links along its circumference such that its exponent becomes $\theta = d\nu - (n - 1)$. Note that in 2D, the Round Table configuration corresponds to the leading order behaviour of a composite knot. Each fringe loop, that is, corresponds to a prime component. The additional degrees of freedom coming about by the relative motion of the fringe loops in this configuration correspond to the enhancement of accessible numbers of configurations for knotted chains as measured by Orlan-dini *et al.* [63, 64].

2. The figure-eight cactus with attached loops

Consider a figure-eight paraknot in which n and m additional (external) loops are attached to the two loops (compare Fig. 3b in which $n = 2$ and $m = 1$). The external loops are all strongly localised and give rise to

additional sliding entropy for the figure-eight loops; by choosing different values for n and m , one obtains various localisation properties for the figure-eight loops. For instance, for $n = 2$ and $m = 1$, ℓ_4 is loose and ℓ_5 is weakly localised; for $n, m \geq 2$, both ℓ_4 and ℓ_5 are loose, i.e., proportional to L , so that the gyration radius of the paraknot is smaller than for a simple ring of same length L . In this case, the joint PDF does not factorise, but the scaling function \mathcal{Y}_8 from Eq. (6) enters. Depending on the details of the structure, the gyration radius should be given by similar expressions as developed in Refs. [6, 53]. Note that analogous loosening of loops can be achieved for open paraknots of the type sketched in Fig. 2g.

3. The Necklace

Finally, let us explore the Necklace structure from Fig. 2h whose corresponding arc diagram is shown in Fig. 6b. In this configuration, the two end-loops are strongly localised; the other $m = n - 2$ inner loops have two neighbours. By necessity, one of the inner loops has to be loose (size L), and has sliding entropy with weight $\sim L^{1-d\nu}$. On each side of the large loop there is a number of other inner loops, arranged in a hierarchy of shapes of the type .oOoo. (. = strongly localised end-loop, o = weakly localised loop, O = large inner loop), statistically changing to .oooO. etc. If one focuses on one particular inner loop, there is a $1/m$ chance to find this loop large with the (integrated) PDF $\sim L^{1-d\nu}$. Note that a complete analysis of this relatively simple and symmetric structure is already quite nontrivial.

The Necklace structure can be closed by an additional slip-link connecting the two outer loops. This forms a symmetric configuration in which all loops are *a priori* equivalent. This paraknot is equal to the network studied for flat prime knots in Ref. [61]. Accordingly, the closed Necklace structure is, to leading order, contracted to the figure-eight paraknot in both 2D and 3D.

V. CONCLUSIONS

We have presented a systematic study of slip-link structures which we call paraknots. Paraknots are relatively easy to deal with analytically and may provide information on the generic interplay between entropy and fixed topology in polymer chains and networks.

Paraknots composed of ideal chains are described by Gaussian propagators for which calculations are reasonably straightforward. Simple paraknots in 2D and 3D are only marginally or weakly localised whereas localisation is strong in higher dimensions. More complicated paraknots in which individual loops are connected to more than one slip-link show less localisation due to the additional degrees of freedom brought about by the rela-

tive motion of the slip-links or additional sliding-rings on a loop. If self-avoiding effects are considered, simple paraknots are strongly localised even in 2D and 3D. The scaling exponents involved can be obtained from Duplantier's theory for general polymer networks. For the figure-eight paraknot, we have confirmed the scaling exponent through Monte Carlo simulations. Localisation in self-avoiding paraknots becomes weakened if more than one substructure has additional degrees of freedom, in analogy to the ideal chain case. This observation pertains to arbitrary topological polymer networks.

The tightness of paraknots in 2D quantifies the strong localisation for flat knots observed by Guitter and Orlandini [64]. Whereas we cannot infer definitive statements on 3D knots from our analysis, the correspondence between figure-eight paraknot and the leading order behaviour of prime knots (and between the Round Table configuration and composite knots) in 2D suggests that similar tightness could be observed in 3D as well. This is consistent with the findings of Janse van Rensburg and Whittington [62], Orlandini *et al.* [63] and Katritch *et al.* [65], and it differs from the conclusions of Quake [53].

Additional energetic effects due to bending and the presence of (screened) electric charges are relevant for many systems, especially in biology. In so far as these effects can be accommodated by the introduction of a persistence length, they should not affect our results in the long-chain limit. However, they determine the crossover size for the onset of the long-chain limit in the polymer. For the particular case of the 2D trefoil knot the results of our previous analysis suggest that the continuum limit is reached for chains with 512 monomers, whereas for the figure-eight paraknot even chain lengths of 128 seem to be sufficient. Thus, in a DNA double helix for which the persistence length is of the order of 100 base pairs (bp), one may expect to see localisation behaviours in *simple* topologically entangled states for strand lengths of the order of 10 to 50 kbp, corresponding to a length of 5 to $25\mu\text{m}$ [77]. For shorter DNA strands, it is to be expected that finite size effects prevail, and thus the knots or other topological details will be spread out over a considerably larger part of the entire chain.

Acknowledgments

We acknowledge financial support from the National Science Foundation (DMR-01-18213 and PHY99-07949) and the US-Israel Binational Science Foundation (BSF) grant No. 1999-007. AH and RM acknowledge financial support from the Deutsche Forschungsgemeinschaft (DFG). AH also acknowledges financial support by the Engineering and Physical Sciences Research Council through grant GR/J78327. PGD acknowledges financial support from the Research Council of Norway.

[1] P. J. Flory, *Principles of Polymer Chemistry*, (Cornell University Press, Ithaca, New York, 1953).

[2] P.-G. de Gennes, *Scaling concepts in polymer physics* (Cornell University Press, Ithaca, New York, 1979).

[3] M. Doi and S. F. Edwards *The Theory of Polymer Dynamics* (Clarendon Press, Oxford, 1986).

[4] L. R. G. Treloar, *The physics of rubber elasticity* (Clarendon Press, Oxford, 1975).

[5] J. D. Ferry, *Viscoelastic properties of polymers* (Wiley, New York, 1970).

[6] A. Yu. Grosberg and A. R. Khokhlov, *Statistical Mechanics of Macromolecules* (AIP Press, New York, 1994).

[7] K. Reidemeister, *Knotentheorie* (Springer, Berlin, 1931) [*Knot theory* (BSC Assocs., Moscow, Idaho, 1983)].

[8] L. H. Kauffman, *Knots and physics*, Series on knots and everything, vol. I (World Scientific, Singapore, 1993).

[9] A. C. C. Adams, *The knot book: an elementary introduction to the mathematical theory of knots* (Freeman, New York, 1994).

[10] H. L. Frisch and E. Wassermann, *J. Am. Chem. Soc.* **83**, 3789 (1961); M. Delbrück, in *Mathematical problems in biological sciences* (Proc. Symp. Appl. Math. **14**, 55 (1962)), edited by R. E. Bellman.

[11] D. W. Sumners and S. G. Whittington, *J. Phys. A* **21**, 1689 (1988); N. Pippenger, *Discrete Appl. Math.* **25**, 273 (1989); see also Y. Diao, N. Pippenger and D. W. Sumners, *J. Knot Theory Ramifications* **3**, 419 (1994).

[12] B. Alberts, K. Roberts, D. Bray, J. Lewis, M. Raff and J. D. Watson, *The molecular biology of the cell* (Garland, New York, 1994); S. R. Bolsover, J. S. Hyams, S. Jones, E. A. Shephard and H. A. White, *From Genes to Cells* (Wiley, New York, 1997).

[13] S. A. Wassermann and N. R. Cozzarelli, *Science* **232**, 951 (1986).

[14] S. A. Wassermann and N. R. Cozzarelli, *Proc. Natl. Acad. Sci. USA* **82**, 1079 (1984); S. A. Wassermann, J. M. Dungan and N. R. Cozzarelli, *Science* **229**, 171 (1985).

[15] T. R. Strick, V. Croquette and D. Bensimon, *Nature* **404**, 901 (2000); S. Y. Shaw and J. C. Wang, *Science* **260**, 533 (1993); T. Deguchi and K. A. Tsurusaki, *J. Knot Theory Ramific.* **3**, 321 (1994); S. A. Wasserman, J. M. Dungan and N. R. Cozzarelli, *Science* **229** 171 (1985).

[16] J. Yan, M. O. Magnasco and J. F. Marko, *Nature* **401**, 932 (1999); V. V. Rybenkov, C. Ullsperger, A. V. Vologodskij and N. R. Cozzarelli, *Science* **277**, 690 (1997).

[17] F. Major, D. Gautheret and R. Cedergren, *Proc. Natl. Acad. Sci. USA* **90**, 9408 (1993); J. D. Puglisi, J. R. Wyatt and I. Tinoco, *J. Mol. Biol.* **214**, 437 (1990); *RNA Structure and function* edited by R. W. Simons and M. Grunberg-Manago (Cold Spring Harbor Laboratory Press, New York, 1998).

[18] R. Bundschuh and T. Hwa, *Phys. Rev. Lett.* **83**, 1479 (1999); U. Gerland, R. Bundschuh and T. Hwa, cond-mat/0101250.

[19] D. Poland and H. A. Scheraga, *J. Chem. Phys.* **45**, 1464 (1966); *Theory of Helix-Coil Transitions in Biopolymers* (Academic Press, New York, 1970).

[20] Y. Kafri, D. Mukamel and L. Peliti, *Phys. Rev. Lett.* **85**, 4988 (2000).

[21] Y. Kafri, D. Mukamel and L. Peliti, cond-mat/0108323.

[22] A. Hanke and R. Metzler, cond-mat/0110164.

[23] W. R. Taylor, *Nature* **406**, 916 (2000); M. L. Mansfield, *Nature Struct. Biol.* **1**, 213 (1994); *ibid.* **4**, 116 (1997); F. Takusagawa and K. Kamitori, *J. Am. Chem. Soc.* **118**, 8945 (1996).

[24] T. E. Creighton, *Proteins: structures and molecular properties*, (W. H. Freeman, New York, 1993).

[25] S. Y. Shaw and J. C. Wang, *Science* **260**, 533 (1993); V. V. Rybenkov, N. R. Cozzarelli and A. V. Vologodskij, *Proc. Natl. Acad. Sci. USA* **90**, 5307 (1993); A. Stasiak, V. Katritch, J. Bednar, D. Michoud and J. Dubochet, *Nature* **384**, 122 (1996); A. V. Vologodskij, N. J. Crisponi, B. L. P. Pieranski, V. Katritch, J. Dubochet and A. Stasiak, *J. Mol. Biol.* **278**, 1 (1998); S. Trigueros, J. Arsuaga, M. E. Vazquez, D. W. Sumners and J. Roca, *Nucl. Acids Res.* **29**(13) e67.

[26] C. W. Pouton and L. W. Seymour, *Adv. Drug Delivery Rev.* **46**, 187 (2001); *Protein targeting and translocation*, edited by D. A. Phoenix (Princeton University Press, Princeton, New Jersey, 1998).

[27] H. Fujisawa and M. Morita, *Genes to Cells* **2**, 537 (1997); C. E. Catalano, D. Cue and M. Feiss, *Mol. Microbiol.* **16**, 1075 (1995).

[28] G. Schill, *Catenanes, rotaxanes and knots* (Academic Press, New York, 1971).

[29] J.-M. Lehn *Supramolecular Chemistry* (VCH, Weinheim, 1995).

[30] *Catenanes, Rotaxanes and Knots*, edited by J.-P. Sauvage and C. Dietrich-Buchecker (VCH, Weinheim, 1999).

[31] Single molecule spectroscopy. W. E. Moerner and M. Orrit, *Science* **283**, 1670 (1999); W. E. Moerner and L. Kador, *Phys. Rev. Lett.* **62**, 2535 (1989).

[32] Optomicroscopical imaging. A. van Oudenaarden and J. A. Theriot, *Nat. Cell. Biol.* **1**, 493 (1999); J. A. Theriot, T. J. Mitchison, L. G. Tilney and D. A. Portnou, *Nature* **37**, 257 (1992).

[33] Atomic force microscopy. G. Binnig, C. F. Quate and C. Gerber, *Phys. Rev. Lett.* **56**, 930 (1986).

[34] Optical tweezers. A. Ashkin, *Phys. Rev. Lett.* **24**, 156 (1970); A. Ashkin, J. M. Dziedi and T. Yamane, *Nature* **330**, 769 (1987); M. D. Wang, H. Yin, R. Landeck, J. Gelles and S. M. Block, *Biophys. J.* **72**, 1335 (1997); J.-C. Meiners and S. R. Quake, *Phys. Rev. Lett.* **84**, 5014 (2000).

[35] Y. Arai, R. Yasuda, K.-I. Akashi, Y. Harada, H. Miyata, K. Kinoshita jr. and H. Itoh, *Nature* **399**, 446 (1999).

[36] M. Rief, M. Gautel, F. Oesterhelt, J. M. Fernandez and H. E. Gaub, *Science* **276**, 1109 (1997); U. Bockelmann, B. Evassez-Roulet and F. Heslot, *Phys. Rev. Lett.* **79**, 4489 (1997), *Phys. Rev. E* **58**, 2386 (1998); R. E. Thomson and E. D. Siggia, *Europhys. Lett.* **31**, 335 (1995).

[37] B. Maier and J. O. Rädler, *Phys. Rev. Lett.* **82**, 1911 (1999).

[38] J. Kepler, in W. v. Dyck and M. Caspar (Editors), *Johannes Kepler, Gesammelte Werke* (Beck, München, 1937).

[39] L. Euler *Solutio problematis ad geometriam situs pertinens* Comment. Academiae Sci. Imp. Petropolitanae **8**, 128 (1736); English translation: *Sci. Amer.* **189**, 66 (1953).

[40] J. B. Listing, *Vorstudien zur Topologie*, Göttinger Stu-

dien (Vandenhoeck und Ruprecht, Göttingen, 1848).

[41] W. Thomson, Lord Kelvin, Phil. Mag. **34**, 15 (1867); Proc. Roy. Soc. Edinburgh 1875-76, p. 59.

[42] http://www-groups.dcs.st-and.ac.uk/~history/HistTopics/Knots_and_physics.html.

[43] P. G. Tait, Trans. Roy. Soc. Edinburgh **28**, 145 (1876-7); *ibid.*, **32**, 327 (1883-4); *ibid.*, **32**, 493 (1884-5); *Scientific papers* (Cambridge University Press, London, 1898).

[44] T. P. Kirkman, Proc. Royal Soc. Edinburgh **13**, **120**, 363 (1884-5); *ibid.*, **32**, 483 (1884-5).

[45] C. N. Little, Trans. Connecticut Acad. Sci. 18, **7**, 27 (1885); Trans. Roy. Soc. Edinburgh **35**, 771 (1890); *ibid.* **36**, 253 (1890-1).

[46] T. A. Vilgis, Phys. Rep. **336**, 167 (2000).

[47] A. L. Kholodenko and T. A. Vilgis, Phys. Rep. **298**, 251 (1998).

[48] For comparison, self-avoidance in 3D is usually treated as a perturbation, i.e., as a “soft constraint”, in analytical studies [2].

[49] S. F. Edwards, Proc. Phys. Soc. **91**, 513 (1967); J. Phys. A **1**, 15 (1968).

[50] P.-G. de Gennes, Macromol. **17**, 703 (1984).

[51] M. Otto and T. A. Vilgis, Phys. Rev. Lett. **80**, 881 (1998).

[52] A. Yu. Grosberg, Phys. Rev. Lett. **85**, 3858 (2000).

[53] S. R. Quake, Phys. Rev. Lett. **73**, 3317 (1994); Phys. Rev. E **52**, 1176 (1996).

[54] A. Yu. Grosberg, A. Feigel and Y. Rabin, Phys. Rev. E **54**, 6618 (1996).

[55] M. E. Cates and J. M. Deutsch, J. Phys. (Paris) **47**, 2121 (1986); M. Müller, J. P. Wittmer and M. E. Cates, Phys. Rev. E **53**, 5063 (1996); *ibid.* **61**, 4078 (2000).

[56] A. Grosberg and S. Nechaev, J. Phys. A **25**, 4659 (1991).

[57] S. Nechaev, cond-mat/9812205.

[58] M. Doi and S. F. Edwards, J. Chem. Soc. Farad. Trans. **274**, 1802 (1978); R. C. Ball, M. Doi, S. F. Edwards and M. Warner, Polymer **22**, 1010 (1981); P. G. Higgs and R. C. Ball, Europhys. Lett. **8**, 357 (1989); S. F. Edwards and T. A. Vilgis, Polymer **27**, 483 (1986).

[59] B. Erman and J. E. Mark, *Structures and properties of rubberlike networks* (Oxford, New York, 1997).

[60] B. D. Hughes *Random Walks and Random Environments, Volume 1: Random Walks* (Oxford University Press, Oxford, 1995).

[61] R. Metzler, A. Hanke, P. G. Dommersnes, Y. Kantor and M. Kardar, cond-mat/0110266.

[62] E. J. Janse van Rensburg and S. G. Whittington, J. Phys. A **24**, 3935 (1991).

[63] E. Orlandini, M. C. Tesi, E. J. Janse van Rensburg and S. G. Whittington, J. Phys. A **31**, 5953 (1998); compare *ibid.* **29**, L299 (1996).

[64] E. Guitter and E. Orlandini, J. Phys. A **32**, 1359 (1999).

[65] V. Katritch, W. K. Olson, A. Vologodskii, J. Dubochet and A. Stasiak, Phys. Rev. E **61**, 5545 (2000).

[66] M. K. Shimamura and T. Deguchi, Phys. Rev. E **64**, 020801 (2001).

[67] Here and in the following we consider two configurations of a polymer chain different if they cannot be matched by translation. In addition, the origin of a given structure is fixed by a vertex point, i.e., a point where several legs of the polymer chain are joint. For a simply connected ring polymer, such a vertex is a two-vertex anywhere along the chain.

[68] Note that the above factorisation does not take place in structures where additional links are introduced, such as connecting the two corner loops in the necklace configuration sketched in Fig. 2h; this creates conditional probabilities, and the associated arc diagrams no longer correspond to Hartree graphs.

[69] R. Metzler, Y. Kantor and M. Kardar (unpublished).

[70] B. Duplantier, Phys. Rev. Lett. **57**, 941 (1986); J. Stat. Phys. **54**, 581 (1989).

[71] L. Schäfer, C. v. Ferber, U. Lehr and B. Duplantier, Nucl. Phys. B **374**, 473 (1992).

[72] K. Ohno and K. Binder, J. Phys. (Paris) **49**, 1329 (1988).

[73] B. Nienhuis, Phys. Rev. Lett. **49**, 1062 (1982); J. Stat. Phys. **34**, 731 (1984).

[74] M. B. Hastings, Z. A. Daya, E. Ben-Naim, and R. E. Ecke, cond-mat/0110612.

[75] J. des Cloizeaux, J. Phys. (Paris) **41**, 223 (1980).

[76] If the segments $\ell_1, \ell_2, \dots, \ell_M$ are loose, the cutoff a is no longer relevant and characteristic lengths can be calculated by multiple integrals of the form

$$I_j(L) = \int_0^L d\ell_1 \ell_1^{-\theta_1} \dots \int_0^{L-\sum_{i=1}^{j-1} \ell_i} d\ell_j \ell_j^{1-\theta_j} \dots \times \int_0^{L-\sum_{i=1}^{M-1} \ell_i} d\ell_{M-1} \ell_{M-1}^{-\theta_{M-1}} \left(L - \sum_{i=1}^{M-1} \ell_i \right)^{-\theta_M},$$

whose Laplace transform ($L \rightarrow u$)

$$\widetilde{I_j(u)} = u^{\sum_{i=1}^M (\theta_i - 1) - 1} \Gamma(2 - \theta_j) \prod_{i \neq j} \Gamma(1 - \theta_i)$$

yields in a simple product form by the integration theorem for the first integral and the convolution theorem for the remaining factors, and therefore

$$I_j(L) = L^{\sum_{i=1}^M (1 - \theta_i)} \frac{\Gamma(2 - \theta_j) \prod_{i \neq j} \Gamma(1 - \theta_i)}{\Gamma(1 + \sum_{i=1}^M [1 - \theta_i])}.$$

With similar expressions for the normalisation, one obtains the results quoted in the text.

[77] J. F. Marko and E. D. Siggia, Macromol. **28**, 8759 (1995).